The Reaction of Phenyl Radical with Molecular Oxygen: A G2M Study of the Potential Energy Surface

Igor V. Tokmakov,[†,||] Gap-Sue Kim,[‡,¶] Vadim V. Kislov,[§,#] Alexander M. Mebel,[*,§] and Ming C. Lin[*,†]

Department of Chemistry, Emory University, Atlanta, Georgia 30322,Institute of Atomic and Molecular Sciences, Academia Sinica, P.O. Box 23-166, Taipei 10764, Taiwan, and Department of Chemistry and Biochemistry, Florida International University, Miami, Florida 33199

Received: April 4, 2005

Ab initio G2M calculations have been performed to investigate the potential energy surface for the reaction of C_6H_5 with O_2. The reaction is shown to start with an exothermic barrierless addition of O_2 to the radical site of C_6H_5 to produce phenylperoxy (**1**) and, possibly, 1,2-dioxaspiro[2.5]octadienyl (dioxiranyl, **8**) radicals. Next, **1** loses the terminal oxygen atom to yield the phenoxy + O products (**3**) or rearranges to **8**. The dioxiranyl can further isomerize to a seven-member ring 2-oxepinyloxy radical (**10**), which can give rise to various products including $C_5H_5 + CO_2$, pyranyl + CO, *o*-benzoquinone + H, and 2-oxo-2,3-dihydrofuran-4-yl + C_2H_2. Once **10** is produced, it is unlikely to go back to **8** and **1**, because the barriers separating **10** from the products are much lower than the reverse barrier from **10** to **8**. Thus, the branching ratio of $C_6H_5O + O$ against the other products is mostly controlled by the critical transition states between **1** and **3**, **1** and **8**, and **8** and **10**. According to the calculated barriers, the most favorable product channel for the decomposition of **10** is $C_5H_5 + CO_2$, followed by pyranyl + CO and *o*-benzoquinone + H. Since $C_6H_5O + O$ and $C_5H_5 + CO_2$ are expected to be the major primary products of the $C_6H_5 + O_2$ reaction and thermal decomposition of C_6H_5O leads to $C_5H_5 + CO$, cyclopentadienyl radicals are likely to be the major product of phenyl radical oxidation, and so it results in degradation of the six-member aromatic ring to the five-member cyclopentadienyl ring. Future multichannel RRKM calculations of reaction rate constants are required to support these conclusions and to quantify the product branching ratios at various combustion conditions.

Introduction

The reaction of phenyl radical (C_6H_5) with O_2 is of great importance in the chemistry of incipient soot formation and also in combustion of aromatic hydrocarbons, which represent important ingredients of lead-free gasoline.[1−3] At high temperatures, phenyl radical can be either oxidized through the $C_6H_5 + O_2$ reaction or undergoes the polymerization process, $C_6H_5 + nC_2H_2 \rightarrow$ polyaromatic hydrocarbons (PAHs), which are the building blocks of soot particles in hydrocarbon combustion[1,4] or subjected to thermal decomposition to smaller fragments. The competition of these two processes effectively determines the amount of soot produced in combustion, and therefore it is critical to know their mechanisms, rate constants, and relative product yields under varying combustion conditions, such as the temperature and pressure. At $T \geq 1000$ K, the $C_6H_5 + O_2$ reaction is believed to occur primarily via the metathetical process

$$C_6H_5 + O_2 \rightarrow C_6H_5O + O$$

leading to the formation of a phenoxy radical which then can fragment yielding the $C_5H_5 + CO$ products above 900 K.[5,6] Other minor reaction channels producing H atoms and *o*- and *p*-benzoquinone have also been invoked:[7]

$$C_6H_5 + O_2 \rightarrow o/p\text{-}C_6H_4O_2 + H$$

Under low temperatures, the reaction has been shown to proceed by the addition-stabilization process leading to the phenylperoxy radical (**1**):[8]

$$C_6H_5 + O_2 \rightarrow C_6H_5OO$$

In addition, theoretical calculations[9−12] of the potential energy surface (PES) for the $C_6H_5O_2$ system showed that, in principle, many other reaction products are also possible:

$$C_6H_5 + O_2 \rightarrow C_5H_5 + CO_2$$

$$C_6H_5 + O_2 \rightarrow C_5H_5O \text{ (pyranyl)} + CO$$

$$C_6H_5 + O_2 \rightarrow C_4H_3O_2 + C_2H_2$$

To predict reliable reaction rate constants and product branching ratios, which can be subsequently used in kinetic modeling of hydrocarbon combustion (oxidation versus incipient soot formation), it is critical to generate an accurate and reliable PES for the $C_6H_5 + O_2$ reaction. Although several attempts to achieve this goal have been made in the recent decade,[9−12] the $C_6H_5O_2$ PESs published so far in the literature are either not complete or lack the desired accuracy and reliability. For

* Authors to whom correspondence should be addressed. E-mail: chemmcl@emory.edu (M.C.L.); mebela@fiu.edu (A.M.M.).
† Emory University.
‡ Academia Sinica.
§ Florida International University.
|| Present address: University of Missouri-Columbia, Department of Chemistry, 601 S. College Ave., Columbia, MO 65211.
¶ Present address: School of Chemistry, Seoul National University, Seoul 151-147, Korea.
# Permanent address: Institute of Solution Chemistry of Russian Academy of Sciences, Akademicheskaya St., 1, Ivanovo, 153045, Russia.

10.1021/jp051712k CCC: $30.25
Published on Web 06/18/2005

instance, Carpenter studied some intermediates and transition states for the oxidative cleavage of phenyl radical at the semiempirical PM3 method.[9] Mebel and Lin calculated a variety of the $C_6H_5O_2$ isomers[10] as well as transition states for the $C_6H_5O + O$ reaction[11] using the ab initio PUMP3/6-31G*//UHF/6-31G* method. However, the use of semiempirical and even ab initio Hartree−Fock and perturbation-theory-based methods with a moderate basis set may not provide chemical accuracy for such a complicated open-shell system as $C_6H_5O_2$. The most recent theoretical study of the $C_6H_5O_2$ PES was performed by Fadden et al.[12a] who employed the hybrid density functional B3LYP/6-311+G**//B3LYP/6-31G* method to calculate various intermediates and transition states for unimolecular decomposition pathways of phenylperoxy radical. This group also studied in more detail transformations of the key reaction intermediate, 2-oxepinyloxy radical,[12b] and considered the mechanism of the 2-oxepinyloxy + O_2 reaction.[12c] The results of the DFT calculations may be more accurate than the energetics and molecular parameters calculated earlier, but still, the accuracy expected from the B3LYP method for the relative energies of intermediates and for the barrier heights is not sufficient to generate reliable kinetic data, such as rate constants and product branching ratios. Moreover, some of the B3LYP results, for example, the existence of distinct transition states for the $C_6H_5 + O_2 \rightarrow C_6H_5OO$ and $C_6H_5OO \rightarrow C_6H_5O + O$ reaction steps, do not seem to be qualitatively correct and require further investigation employing higher-level theoretical methods. The connections between some transition states and intermediates were not unambiguously confirmed by intrinsic reaction coordinate (IRC) calculations and therefore remain questionable.

Our goal in the present study is to uncover a qualitatively compelling and comprehensive reaction mechanism (in terms of the potential energy surface) and to provide chemically accurate energetics and molecular parameters for various species involved in the reaction of phenyl radical with O_2, which can be subsequently used in multichannel RRKM calculations of temperature- and pressure-dependent rate constants for individual reaction steps and for product branching ratios.

Calculation Methods

The geometries of various reactants, products, intermediates, and transition states in the $C_6H_5 + O_2$ reaction were initially optimized at the hybrid density functional B3LYP/6-31G* level of theory[13] and their vibrational frequencies were then computed using the same method. Because the B3LYP/6-31G* geometries and frequencies were reported previously for some of the structures involved,[12] we have not recomputed them here; the calculations were performed only for the species that were not considered earlier. For intermediates and transition states participating in the most important reaction channels, the geometries were reoptimized and vibrational frequencies were recomputed with a larger basis set, at the B3LYP/6-311++G** level. All connections between transition states and local minima were confirmed by intrinsic reaction coordinate (IRC) calculations.[14]

Next, the relative energies of various species were refined by single-point calculations using the modified Gaussain 2 G2M(MP2) method[15] with the B3LYP/6-31G* or B3LYP/6-311++G** optimized geometries. The total G2M(MP2) energies were computed as follows:

$$E[\text{G2M(MP2)}] = E[\text{CCSD(T)/6-311G(d,p)}] + \Delta E(+3\text{df2p}) + \Delta E(\text{HLC}) + \text{ZPE}$$

where

$$\Delta E(+3\text{df2p}) = E[\text{MP2/6-311+G(3df,2p)}] - E[\text{MP2/6-311G(d,p)}]$$

and zero-point vibrational energy (ZPE) corrections were obtained at either B3LYP/6-31G* or B3LYP/6-311++G** levels of theory. The higher level correction, ΔE(HLC), was not actually used because most of the species involved, except $C_6H_5 + O_2$ and $C_6H_5O + O$, have the same overall doublet multiplicity and therefore the same number of paired and unpaired electrons. If ΔE(HLC) were included, the relative energies of all doublet intermediates, transition states, and products with respect to the $C_6H_5 + O_2$ reactants would have been lowered by ~3 kcal/mol.[15] In the coupled cluster and MP2 calculations, most of the energies were computed from restricted RCCSD(T) and unrestricted UMP2 components, respectively, but in some cases we had to use the unrestricted UCCSD(T) method instead of RCCSD(T) (see Supporting Information). RCCSD(T)[16] here denotes partially spin-adapted open-shell coupled cluster singles and doubles theory augmented with a perturbation correction for triple excitations (the RHF-RCCSD(T) keyword in the MOLPRO program).

A legitimate question that can be raised is whether the single-reference coupled cluster method is able to properly describe the energetics of the $C_6H_5 + O_2$ reaction system. Although the CCSD(T) level has come to be the gold-standard level of theory for single-reference calculations and it is appropriate for calculations of systems with a mild multireference character and is certainly more reliable than the DFT B3LYP method, some caution in interpretation of the results is warranted in cases when the so-called T1 diagnostic values exceed 0.02.[17] As seen in Supporting Information, this indeed is the case for some intermediates and transition states considered in this work. However, at present, unfortunately, a viable and reliable alternative to CCSD(T) calculations does not exist for systems of such size as $C_6H_5 + O_2$. Multireference CASPT2 or MRCI methods with large and flexible basis sets, which take into account both nondynamical and dynamical contributions into electron correlation, are in principle more robust than CCSD(T) but only if all valence electrons and valence orbitals are included into the calculations as part of the active space or at least through single and double excitations at the post-CASSCF stage. Otherwise, these methods suffer from the subjectivity in the active space choice and the results appear to be active-space-dependent. The CASPT2 and MRCI energies may be of a rather poor quality if single and double excitations are not included from all valence electrons (beyond the active space) because a large portion of dynamical electron correlation then remains unaccounted for. Ideally, the proper active space for the $C_6H_5O_2$ species would include 41 valence electrons distributed over 37 orbitals. This huge active space can be reduced to a more reasonable size if one includes only those orbitals that are involved in particular bond cleavage/bond formation processes and are important for description of nondynamical electron correlation; they are usually characterized by the orbital occupation numbers in the CASSCF wave function ranging from 1.98 to 0.02. However, even with a smaller active space, all 41 valence electrons need to be subjected to single and double excitations in CASPT2 or MRCI calculations to properly describe dynamical electron correlation, which, unfortunately, is unfeasible in the foreseeable future. To evaluate the expected accuracy of our calculations, we compared our results for $C_6H_5 + O_2$ with its smaller analogue, the $C_2H_3 + O_2$ reaction system, for which sensible CASPT2 and MRCI calculations are possible.

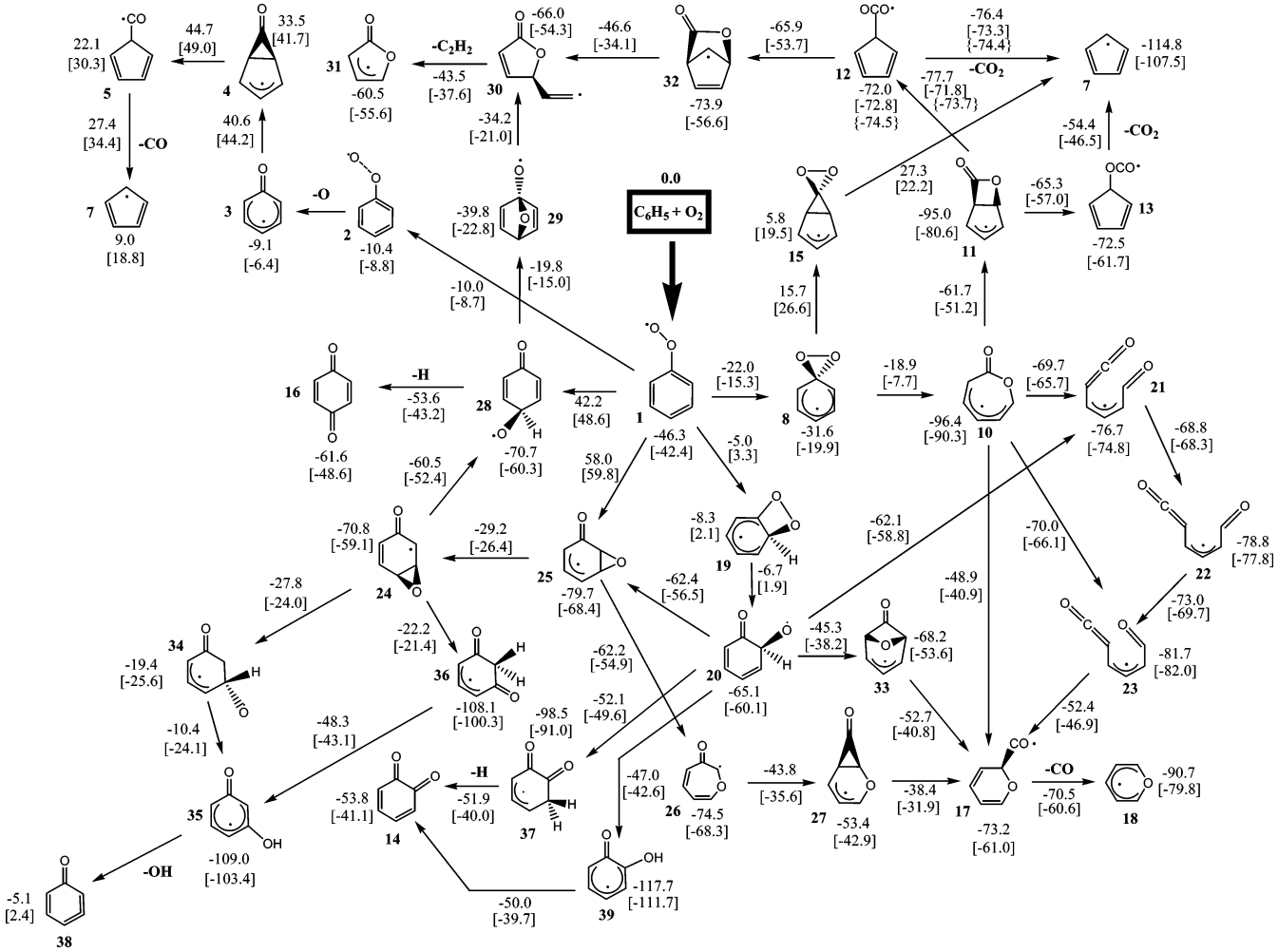

Figure 1. A graph of possible pathways on the global potential energy surface of the $C_6H_5 + O_2$ reaction. Relative energies of the reactants, products, intermediates, and transition states are given in kcal/mol as calculated at the G2M and B3LYP/6-311++G** (in brackets) levels.

CCSD(T) (or G2M) predictions were in a reasonably good agreement with MRCI results (on the basis of our limited comparison) for $C_2H_3O_2$, which is prototypical of the present $C_6H_5O_2$. An important factor in choosing the CCSD(T) methodology is that it can be applied uniformly to study various transformations on the $C_6H_5O_2$ PES. Further refinement can be done in future studies by multireference methods with properly constructed active spaces. T1 diagnostic values are provided as indicators of possible importance of multireference effects for proper description of specific intermediates and transition states.

The calculations were carried out using GAUSSIAN 98,[18] Gaussian 03,[19] and MOLPRO 2002[20] quantum chemical program packages. All optimized geometries (Cartesian coordinates), moments of inertia, vibrational frequencies, and total and relative energies calculated by different theoretical methods are collected in the Supporting Information.

Results and Discussion

The $C_6H_5 + O_2$ reaction channels considered in the present study are illustrated in Figure 1. In our discussion, we mostly concentrate on the results, which are qualitatively or quantitatively different from those reported by Fadden et al.[12] We analyze various competitive reaction mechanisms with the goal to select the reaction scheme which includes the most important channels but is feasible for the upcoming multichannel RRKM calculations of the rate constants and product branching ratios.

Entrance Reaction Channel. The reaction starts with addition of the oxygen molecule to the radical site of C_6H_5. As a result, two different isomers of the $C_6H_5O_2$ species can be produced, phenylperoxy radical **1** and dioxiranyl radical **8**, in which the attacked carbon and two oxygen atoms form a three-member ring. Let us first consider the formation of the phenylperoxy radical. The well depth at phenylperoxy is calculated to be 46.3 kcal/mol at the G2M level as compared to the initial reactants. The B3LYP/6-311+G**//B3LYP/6-31G* calculation (with B3LYP/6-31G* ZPE) underestimates this value by 4.0 kcal/mol. Interestingly, the calculated exothermicity of the $C_2H_3 + O_2 \rightarrow$ vinylperoxy radical reaction is rather similar, 46.4 and 41.2 kcal/mol at the G2M and B3LYP/6-311G** levels, respectively.[21] At the B3LYP/6-31G* level, Fadden et al.[12] were able to locate a transition state separating the $C_6H_5 + O_2$ reactants and structure **1**. However, single-point B3LYP/6-311+G**//B3LYP/6-31G* calculations gave the energy of that transition state as −0.2 kcal/mol with respect to the reactants, indicating that a barrier on the reaction pathway is not likely to exist. No barrier was found earlier for the related O_2 addition to C_2H_3 to produce the vinylperoxy radical.[21] To investigate more carefully whether a barrier on the $C_6H_5 + O_2 \rightarrow$ **1** pathway does or does not exist, we calculated the PES profile between the reactants and phenylperoxy radical using partial geometry optimization. In these calculations, the length of the forming C−O bonds was kept fixed at various values

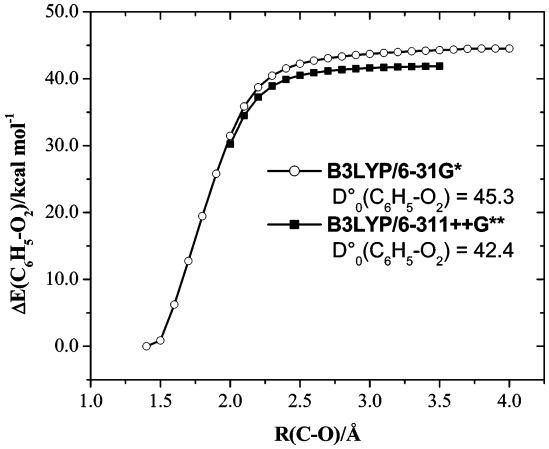

Figure 2. The $C_6H_5-O_2$ dissociation potential energy profiles (ZPE corrected, $T = 0$ K) calculated using the B3LYP density functional with the 6-31G* and 6-311++G** basis sets.

from 4.0 to 1.5 Å, while all other geometric parameters were optimized. The partial optimization calculations were performed at the B3LYP/6-311++G** level within C_s symmetry where the symmetry plane contains all atoms in the molecule. Within the C_s symmetry point group, both the separated reactants and intermediate **1** have the same $^2A''$ electronic state, so that the O_2 addition to the phenyl radical is symmetry-allowed. As seen from the plot of the potential energy curve against the length of the forming C−O bond shown in Figure 2, the energy monotonically and smoothly decreases as the O_2 molecule approaches C_6H_5 until the phenylperoxy radical is produced. This result confirms that no distinct transition state exists on the $C_6H_5 + O_2 \rightarrow$ **1** reaction pathway, at least at the level of theory used in the present study. The reaction rate for the O_2 addition will be controlled by a variational transition state, the position of which and the free-energy barrier will depend on the reaction temperature. We shall discuss the variational transition-state structure and energy as well as the rate constant for the O_2 addition to the phenyl radical and its temperature dependence in a future study. At this point, we conclude that the $C_6H_5 + O_2 \rightarrow$ **1** reaction is barrierless.

Alternatively, the O_2 addition can lead to the formation of the dioxiranyl radical **8**. The latter lies 31.6 kcal/mol lower in energy than the $C_6H_5 + O_2$ reactants at the G2M level. At B3LYP/6-311+G**//B3LYP/6-31G*, the relative energy of **8** was earlier calculated to be −19.9 kcal/mol,[12] so the difference between the DFT and the most accurate G2M values exceeds 10 kcal/mol. The dioxiranyl radical has a C_{2v}-symmetric structure, with the planes containing the six- and three-member rings perpendicular to each other, and the $^2B_1$ electronic state. With the same C_{2v} symmetry point group, the electronic state of the separated C_6H_5 and O_2 reactants is $^2B_2$, which makes the reaction forbidden within C_{2v} symmetry. However, if the symmetry breaks, the oxygen molecule may, in principle, attach to C_6H_5 forming **8** without any barrier. If O_2 approaches the phenyl radical asymmetrically and out-of-plane, some trajectories may, in principle, bypass the transition state separating intermediates **1** and **8** and go directly to **8**. When we tried to locate an asymmetric transition state connecting the reactants with **8**, the search did not result in any saddle-point structure but led to the $C_6H_5 + O_2$ dissociation. However, the possibility of the direct barrierless formation of dioxiranyl from the reactants is only hypothetical at this stage; ab initio molecular dynamics (MD) simulations have to be carried to confirm that such trajectories from $C_6H_5 + O_2$ to **8** actually exist and to evaluate their importance.

Formation and Decomposition of Phenoxy Radical. After the phenylperoxy radical **1** is produced, it can undergo a cleavage of the O−O bond and decompose to the phenoxy radical, C_6H_5O, and to the ground-state oxygen atom, $O(^3P)$. The ground electronic state of C_6H_5O is $^2B_1$ corresponding to $^2A''$ if symmetry is reduced to C_s. Therefore, the overall symmetry of the combined electronic wave function for separated $C_6H_5O(^2B_1) + O(^3P)$ within the C_s point group can be A′ or A″, if the out-of-plane p_z orbital on the oxygen atom is singly or doubly occupied, respectively. It appears that the A′ electronic state is more favorable at long (but finite) separations, and we were able to locate a van der Waals complex **2** between the phenoxy radical and oxygen atom (see Figure 3), which has C_s symmetry and the $^2A'$ electronic state. At the G2M level, the complex is bound by merely 1.3 kcal/mol relative to $C_6H_5O + O$ and lies 35.9 kcal/mol higher in energy than the intermediate **1**. Since the electronic state of the phenylperoxy radical is $^2A''$, the **1** → **2** rearrangement is symmetry-forbidden and can occur only if symmetry is broken. We carefully scanned PES between structures **1** and **2** without symmetry constraints using the O−O distance as the fixed parameter with optimization of all the other internal coordinates. This was followed by a transition-state search, which resulted in TS1−2 shown in Figure 3. As expected, the transition state has a nonplanar geometry with the departing oxygen atom located somewhat above the C_6H_5O plane, where the dihedral OOCC angle τ is −31.9° and −49.4° at the B3LYP/6-31G* and B3LYP/6-311++G** levels of theory, respectively. The O−O distance in TS1−2 is also rather sensitive to the basis set used and decreases from 2.34 to 2.21 Å in going from 6-31G* to 6-311++G**. The optimized structure of the complex **2** is less dependent on the basis set, with the O−O distance varying only from 2.39 to 2.40 Å. In terms of the O−O bond lengths, TS1−2 is a late transition state in both approximations, but it has a much earlier character with the larger basis set. Meanwhile, the pathway for the departure of atomic oxygen from the phenylperoxy radical to form C_6H_5O is rather peculiar. Initially, while the IRC path is climbing from intermediate **1** to TS1−2, the terminal oxygen atom leaves the molecular plane. After the barrier is cleared, the O−O distance continues to increase, but the O atom eventually returns to the C_6H_5O plane and the IRC path descends to the C_s-symmetric (planar) van der Waals complex **2**. Further increase of the O−O distance leads to decomposition of **2** to the phenoxy radical + O. Transition-state TS1−2 resides 10.0 kcal/mol below the initial $C_6H_5 + O_2$ reactants and is 36.3 and 0.4 kcal/mol higher in energy than intermediates **1** and **2**, respectively, but 0.9 kcal/mol lower in energy than the products $C_6H_5O + O$. Experimental heat of formation for the phenylperoxy radical is not available, but we can compare with experiment the calculated heat of the $C_6H_5 + O_2 \rightarrow C_6H_5O + O$ reaction. The agreement is quite close both at the G2M and B3LYP/6-311+G**//B3LYP/6-31G* level, −9.1 and −6.3[12] kcal/mol, respectively, versus −8.2 ± 2.0 in experiment.[22]

Earlier results by Fadden et al.[12] for TS1−2 (TS1−3 in their study) appear to be not reliable. The transition state for the O atom loss from **1** was calculated to be 52.4 and 10.1 kcal/mol higher in energy than the phenylperoxy radical and phenoxy + O products, respectively. Thus, the error in the forward barrier height was about 16 kcal/mol as compared to the present G2M result. The origin of such deviation is not in the use of the B3LYP method, because the present B3LYP/6-311++G** calculations give the barrier at TS1−2 as 33.7 kcal/mol, reasonably close to the G2M value. Instead, Fadden et al.

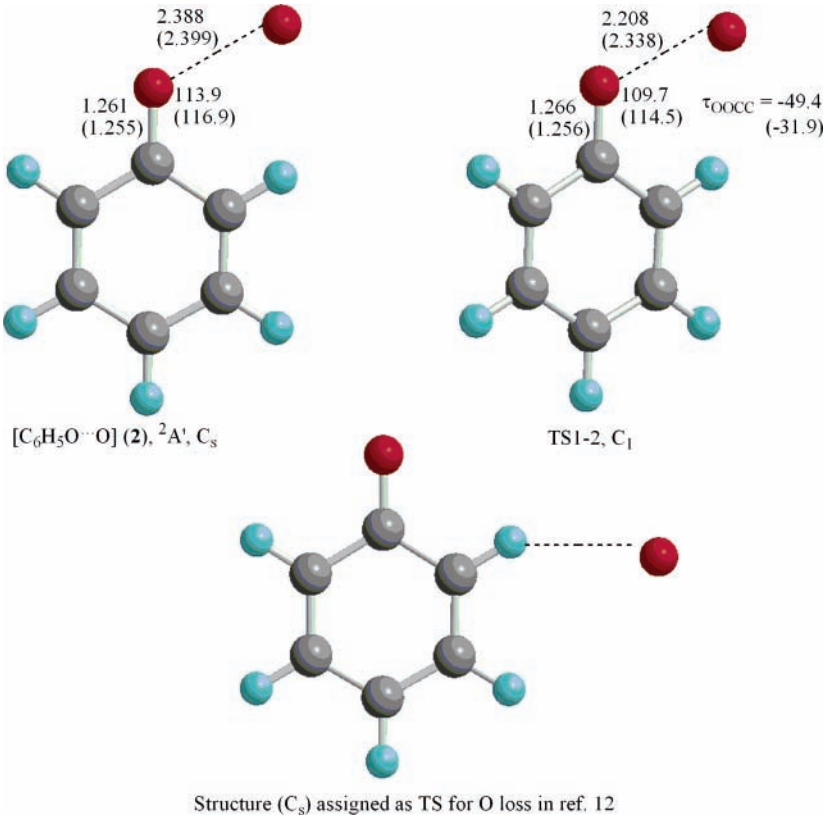

Figure 3. Optimized geometric structures of the van der Waals [$C_6H_5O\cdots O$] complex (**2**) and transition-state TS1−2 separating this complex from the phenylperoxy radical C_6H_5OO (**1**). Selected geometric parameters are shown (bond lengths in Å, bond angles and dihedral angles in degrees) as calculated at the B3LYP/6-311++G** and B3LYP/6-31G* (in parentheses) levels of theory.

apparently have not located the correct geometry for the O-loss transition state; the structure reported in their work is rather different from TS1−2 found here, as it is nearly planar and the dissociating oxygen is positioned closer to one of the CH groups than to the second O atom (see Figure 3).

It is worth noting again the similarity between the C_2H_3OO (vinylperoxy)[21] and C_6H_5OO (phenylperoxy) systems. On the dissociation pathway of C_2H_3OO to $C_2H_3O + O$, the transition state lies 38.6 kcal/mol above the initial intermediate and, after the barrier is cleared, the $C_2H_3O\cdot O$ van der Waals complex is formed, which is stabilized by 5.7 and 4.0 kcal/mol with respect to the transition state and $C_2H_3O + O$, respectively. A minor quantitative difference between the two systems is found in the relative energies of the O−O bond scission transition states with respect to products; the transition state for the vinylperoxy case is 1.7 kcal/mol higher in energy than $C_2H_3O + O$, whereas for phenylperoxy the corresponding transition state is 0.9 kcal/mol lower in energy than $C_6H_5O + O$. In addition, the $C_2H_3O\cdot O$ complex is more strongly bound (by 4.0 kcal/mol) than $C_6H_5O\cdot O$ **2** (only by 1.3 kcal/mol).

Now, we briefly recap the most favorable decomposition mechanism of the phenoxy radical **3**, $C_6H_5O \rightarrow$ TS3−4 → **4** → TS4−5 → **5** → TS5−7 → C_5H_5 (**7**) + CO, which was studied in detail earlier by us and by other groups.[23−28] The first step involves a formation of a fused bicyclic cyclopropanone intermediate **4** (42.6 kcal/mol above **3**) via a 49.7 kcal/mol barrier at the transition-state TS3−4. This is followed by breaking a CC bond of the three-member ring with a barrier of 53.8 kcal/mol relative to **3** (TS4−5), which leads to intermediate **5** residing 31.2 kcal/mol above **3**. Subsequently, **5** loses carbon monoxide to produce the cyclopentadienyl radical **7**. The barrier for the last reaction step is 36.5 kcal/mol with respect to the phenoxy radical, and the C_5H_5 + CO products lie 18.1 kcal/mol higher in energy than C_6H_5O. The second reaction step, **4** → **5**, exhibits the highest barrier of 53.8 kcal/mol with respect to the initial reactant C_6H_5O and is expected to be rate-determining. The present G2M(MP2) relative energies of intermediates and transition states closely agree with the earlier G2M(rcc,MP2*) values.[26] The only notable quantitative change is a slight increase of the rate-limiting barrier at TS3−4 from 52.2 kcal/mol at G2M(rcc,MP2*) to 53.8 kcal/mol at G2M(MP2). In our previous study,[26] we have also found that RCCSD(T) and CASPT2 relative energies[27] with the same 6-31G** basis are similar in this system indicating that the coupled-cluster method, which is in the base of G2M calculations, properly accounts for nondynamical correlation effects.

Oxygen Insertion into the Benzene Ring. Instead of losing the terminal O atom, the phenylperoxy radical **1** can undergo various rearrangements, which can eventually lead to different reaction products. We start from considering the reaction mechanisms involving insertion of an oxygen atom into the aromatic ring. First, **1** can isomerize to the dioxiranyl radical **8** through a closure of the three-member COO ring, overcoming a barrier of 24.3 kcal/ mol at TS1−8. The barrier height calculated for this process is again similar to the COO ring-closure barrier in the C_2H_3OO system, 25.0 kcal/mol at the same G2M level of theory.[21] Next, one of the oxygens inserts into the ring to produce 2-oxepinyloxy radical (**10**), which contains six carbon atoms and one oxygen atom forming a seven-member ring, with the second O attached to one of the two C atoms adjacent to the ring oxygen. This rearrangement is rather complicated and deserves a detailed consideration. Fadden et al.[12] have found an intermediate structure **9** (see Figure 4) lying between **8** and **10**, but the calculated energy of TS9−10 connecting **9** and **10** was lower than that of **9** even without ZPE corrections at the B3LYP/6-31G* level, at which these stationary

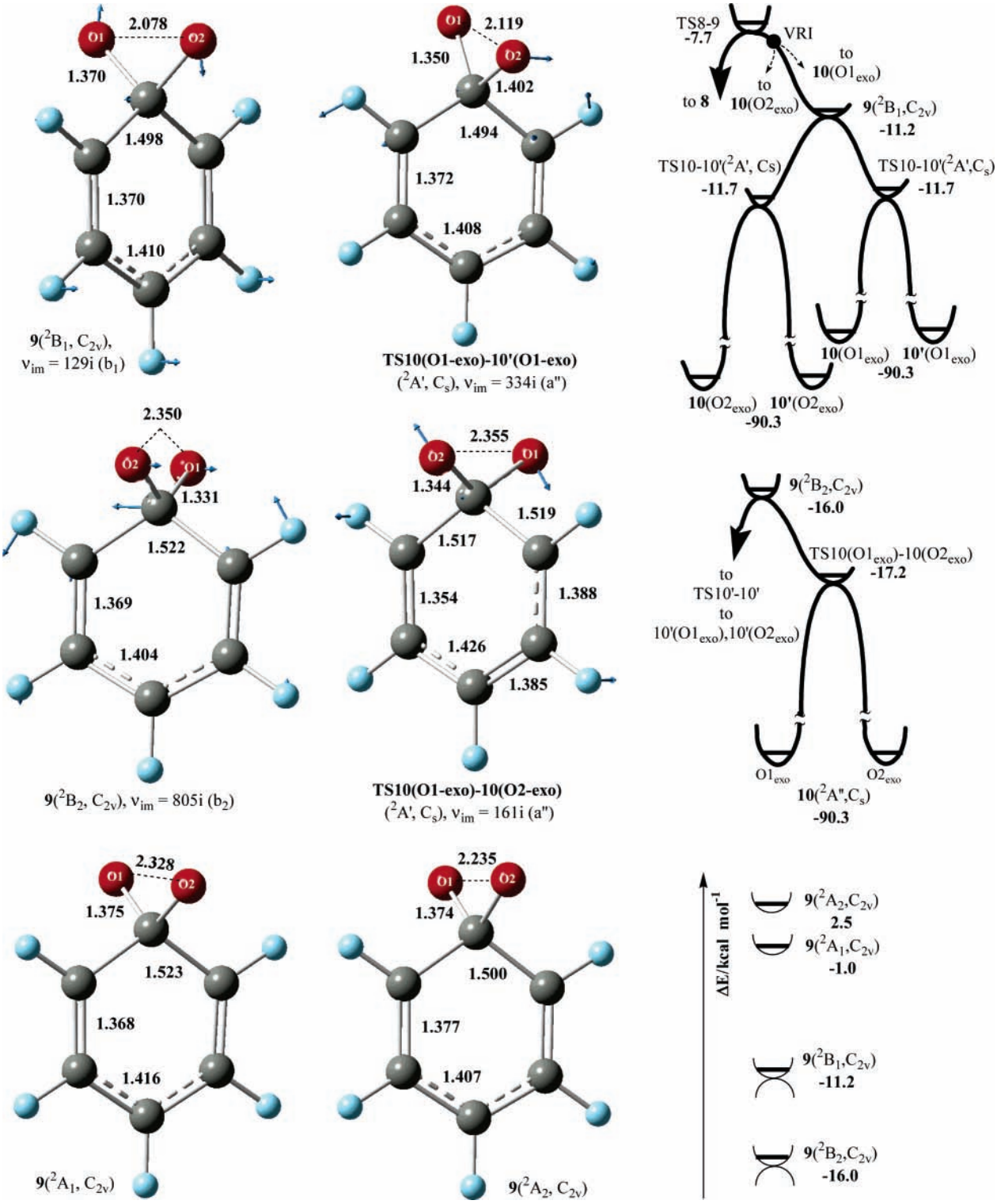

Figure 4. Molecular structures and energetics of the open-shell radical **9** in different doublet electronic states optimized by the B3LYP/6-311++G** method with symmetry constraints. Schematic IRC pathways illustrate connections from the $^2B_1$ and $^2B_2$ states of radical **9** to intermediate **10**. All energies are in kcal/mol relative to $C_6H_5 + O_2$. VRI denotes a valley-ridge inflection point.

structures were optimized. This means that TS9−10 actually cannot connect **9** and **10** and should correspond to another rearrangement. IRC calculations for TS9−10 performed at the B3LYP/6-31G* level showed that TS9−10 connects intermediate **10** with itself (more precisely, with its mirror image **10′** with respect to the plane perpendicular to the molecular plane) and should be denoted as TS10−10′. During the rearrangement involving this TS10−10′, the ring O atom, say, on the right, leaves the molecular plane, rotates about the exocyclic CO bond, and eventually inserts into the adjacent C−C bond on the left, just forming the structure **10′** equivalent to **10**. Interestingly, TS10−10′ has C_s symmetry, but the mirror plane is perpendicular to the ring and contains the CO_2 group.

Intermediate **9** has a molecular structure similar to that of the dioxiranyl radical **8**, but with the O−O bond cleaved. From the electronic structure point of view, **9** can be characterized as a triradical, since it has three low-spin coupled ($2\alpha + 1\beta$) unpaired electrons. Two of those are centered on two oxygen

atoms and the third electron belongs to the π-system of the C_6 ring. Like **8**, **9** has C_{2v} symmetry, but because of the presence of three nearly degenerate singly occupied orbitals, **9** may have several low-lying electronic states, different in symmetry but close in energies.[29]

We need to determine first what electronic state of **9** lies on the reaction path from **8** to **10**. The electronic state of intermediate **8** is $^2B_1$. A search of a transition state for the O−O bond cleavage in **8** gives TS8−9, which is also C_{2v}-symmetric with the $^2B_1$ electronic state. IRC calculations for TS8−9 in the reverse direction confirm the connection of this transition state with intermediate **8**, and in the forward direction these calculations naturally give a stationary point **9** in the same $^2B_1$ state (Figure 4). However, the vibrational frequency analysis of **9**($^2B_1$) shows that it has one imaginary frequency of 181*i* cm^{-1}. As seen in Figure 4, a motion along the eigenvector corresponding to this imaginary frequency breaks C_{2v} symmetry and maintains only C_s symmetry, with the mirror plane perpendicular to the ring and containing the CO_2 fragment and the CH group located at the opposite side of the ring. IRC calculations starting from **9**($^2B_1$) both in forward and reverse directions lead to TS10−10′ (C_s, $^2A'$), which in turn has one imaginary frequency with the eigenvector directed out of the symmetry plane.

As we have already discussed above, IRC calculations for TS10−10′ converge to the equivalent forms of intermediate **10** in both directions; the forward and reverse local minima differ only by the left or right positions of the ring oxygen with respect to the exocyclic C═O bond. The potential energy profile shown in Figure 4 illustrates that **9**($^2B_1$) represents a transition state connecting four equivalent structures **10**, which could be distinguished from one another only if two O atoms and the left and right positions of one of them in the ring were distinguishable. We can also see that transition-state TS8−9 connects local minima **8** and **10**, while the detailed reaction pathway is the following: **8** → (up in energy) → TS8−9 → (down in energy) → **9**($^2B_1$) → (down in energy) → TS10−10′ → (down in energy) → **10**. Despite an apparent complexity of this reaction path, the only fact, which matters for the kinetics of this rearrangement, is that the transition-state TS8−9 connects intermediate **8** with intermediate **10**. This conclusion is confirmed by calculations of vibrational frequencies for points along the IRC for TS8−9, which indicate that there is a valley-ridge inflection point (VRI) less than 5 pm/amu$^{0.5}$ away from TS8−9 in the forward direction. The rest of the IRC calculation in the forward direction follows a ridge all the way to **9**($^2B_1$) while the valleys near this ridge go directly to different forms of **10**.

The $^2B_1$ state is not the lowest electronic state of **9**. An optimization of the $^2B_2$ electronic state gives a structure **9**($^2B_2$) with an energy 4.8 kcal/mol lower (at the B3LYP/6-31++G** level) than that of **9**($^2B_1$). However, **9**($^2B_2$) has two imaginary frequencies at the B3LYP/6-31G* level of theory and one imaginary frequency at B3LYP/6-311++G**. Lowering the symmetry constraints and using B3LYP/6-311++G** IRC calculations (see Figure 4), we were able to follow a continuous descent from **9** (C_{2v}, $^2B_2$) to another stationary point, TS10($O1_{exo}$)−10($O2_{exo}$) (C_s, $^2A'$). TS10($O1_{exo}$)−10($O2_{exo}$) again is not a local minimum but a transition state with one imaginary frequency. This structure has the symmetry plane passing through the ring and reflecting the two oxygen atoms, and the imaginary frequency vibration moves the O atoms in opposite directions destroying C_s symmetry. IRC calculations for TS10($O1_{exo}$)−10($O2_{exo}$) show that this transition state connects two equivalent forms of **10** with interchanged O-atoms, for example, the exocyclic O1 atom in the reactant form becomes endocyclic in the product form, while the endocyclic O2 atom moves in the opposite direction to the exocyclic position.

We have also optimized two other possible electronic states of **9**, $^2A_1$ and $^2A_2$. The optimized structures for these states appeared to be true local minima without imaginary frequencies, but they, respectively, lie 15.0 and 18.5 kcal/mol above **9**($^2B_2$) at the B3LYP/6-31++G** level. The **9**($^2A_1$) structure was actually reported by Fadden et al.[12] We can conclude here that the $^2B_2$, $^2A'$, $^2A_1$, and $^2A_2$ electronic states of **9** are not involved in the **8** → **10** rearrangement and that only the $^2B_1$ state represents a stationary point (though not a local minimum or a critical transition state) on the pathway of oxygen insertion into the benzene ring.

Now, when we have established the mechanism for the oxygen insertion into the aromatic ring, we can look more closely at the energetics of this process. The barrier calculated for the **8** → **10** process is 12.7 kcal/mol, as the corresponding transition-state TS8−9 resides 18.9 kcal/mol below the initial reactants at the G2M level. This barrier is 3.1 kcal/mol higher than the barrier at TS1−8 for the reverse **8** → **1** isomerization (opening of the three-member COO ring). The relative energies of TS1−8 and TS8−9 are critical for the reaction mechanism, since the insertion of the oxygen atom into the ring may lead to several various reaction products, as will be described below, whereas the reverse **8** → **1** rearrangement may be followed by the oxygen loss resulting in the C_6H_5O + O and, eventually, the C_5H_5 + CO + O products. We can compare the present results for the C_6H_5/O_2 system with the corresponding barrier heights for C_2H_3/O_2.[21] For the latter, the barriers for the three-member COO ring opening and for the insertion of the oxygen atom into the C═C bond of the vinyl fragment (passing through a metastable intermediate with O bridging the C−C bond) were earlier calculated at the G2M level to be 16.9 and 24.0 kcal/mol as compared to 9.6 and 12.7 kcal/mol, respectively, for C_6H_5/O_2. We can see that in the phenyl system both barriers decrease, their relative order remains the same, and the difference in the barrier heights decreases from 7.1 kcal/mol for C_2H_3/O_2 to 3.1 kcal/mol for the present system. This may have some implications for the temperature-dependent product branching ratios for the phenyl + O_2 reaction. A detailed investigation of this issue requires multichannel RRKM calculations of the reaction rate constant, which will be the subject of our future work.

In a recent publication,[30] Carpenter has questioned the accuracy of the single-reference-based G2M approach for the relative barrier heights in the vinyl + O_2 system. Using the multireference CASPT2 method with the (23,15) active space and pVTZ basis set, he found the barrier for the COO ring opening and for the O insertion into the C═C bond in the C_2H_3/O_2 system to be 11.9 and 12.5 kcal/mol, respectively, so that the difference between them decreases from 7.1 to merely 0.6 kcal/mol when a seemingly more accurate multireference method is employed. Two aspects of these calculations cause some concern. First, although the (23,15) active space is nominally large, it actually includes only three unoccupied molecular orbitals (MOs) and may not be flexible enough. Second, CAPST2 is a perturbation theory method and it is, in general, inferior with respect to the more expensive MRCI methodology.[17,31] Therefore, we recently carried out MRCI calculations for the two transition states in the C_2H_3/O_2 system. A detailed account of this study will be published elsewhere;[32] here, we only briefly mention the most important result. We used a (9,9) active space in our MRCI calculations, which

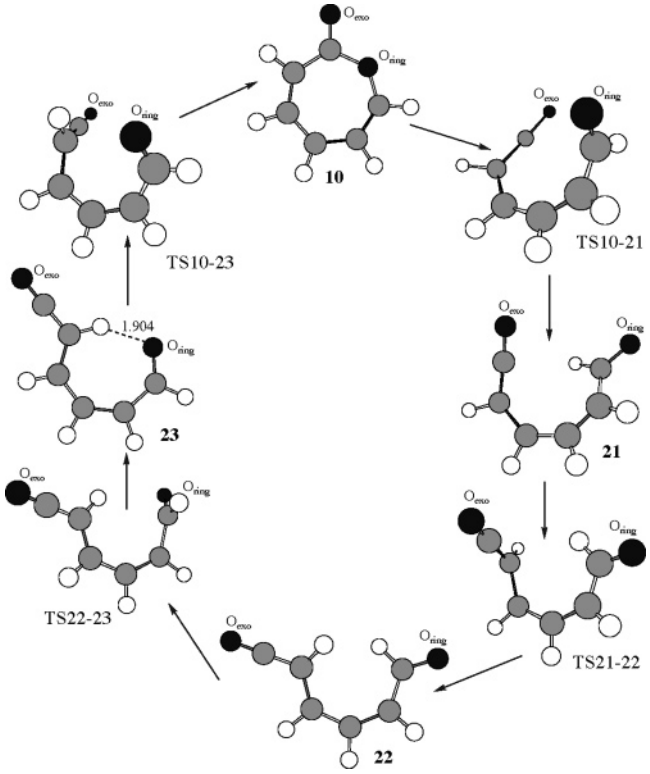

Figure 5. The ring-opening mechanism of the intermediate **10**.

consists of all orbitals having electron populations between 1.98 and 0.02 in the CASSCF wave function. The active space in the initial CASSCF calculations was (9,12), which includes seven unoccupied MOs and is therefore much wider (in terms of the number of configuration state functions, CSFs) than the (23,15) active space used by Carpenter. At the MRCI(9,9)/pVTZ level with Davidson corrections for quadruple excitations, the barriers for the COO ring opening and for the O insertion into the C═C bond are calculated to be 14.5 and 16.9 kcal/mol, respectively. The barrier heights for the O insertion calculated by the MRCI and CCSD(T) methods with the same pVTZ basis set differ only by ∼1 kcal/mol, whereas the value obtained at the CASPT2(9,9)/pVTZ level underestimates the most reliable MRCI result by 6.4 kcal/mol. Unfortunately, meaningful multireference calculations for the C_6H_5/O_2 system with a proper active space are still beyond modern computational facilities and for now we have to rely upon the G2M results keeping in mind their possible inaccuracies illustrated for C_2H_3/O_2. Nevertheless, the multireference effects for TS1−8 and TS8−9 in the C_6H_5/O_2 system are expected to be smaller than for the corresponding transition states in C_2H_3/O_2 because the T1 diagnostic values in CCSD calculations (mean root square of the singles amplitudes)[31] are 0.017 and 0.023 for the former system, notably lower than 0.053 and 0.041 for the latter system, respectively.

Aromatic Ring Opening/Closure and Formation of the C_5H_5O (Pyranyl) + CO Products. The seven-member ring 2-oxepinyloxy radical **10** can undergo ring-opening rearrangements followed by various ring closures eventually leading to a six-member ring intermediate **17** with one oxygen atom within the ring and an out-of-ring CO group. **17** is a precursor of the C_5H_5O (pyranyl) + CO products. The ring-opening processes connecting together intermediates **10**, **21**, **22**, and **23** are illustrated in Figure 5. All of them can be described in terms of rotations of the $C(H)O_{ring}$ and $(H)CCO_{exo}$ fragments around the adjacent C−C bonds. For instance, the isomerization of **10** to **21** occurs by the rotation of the C(H)O group containing the ring oxygen. Once this rotation takes place via TS10−21, the ring C−O bond is broken and an open-chain intermediate **21** is produced. The barrier at TS10−21 is calculated to be 26.7 kcal/mol relative to **10** and the transition state is located 69.7 kcal/mol below the initial reactants. Isomers **10** and **21** lie 96.4 and 76.7 kcal/mol lower in energy than $C_6H_5 + O_2$, respectively. Next, the (H)CCO group in **21**, which contains the oxygen atom formerly being the out-of-ring O_{exo} in **10**, can be rotated leading to another open-chain isomer **22**. The barrier on this pathway is only 7.9 kcal/mol and **22** is 2.1 kcal/mol more favorable than **21**. The next step is again a rotation of the C(H)O group leading to isomer **23** via a low barrier of 5.8 kcal/mol at TS22−23. **23** has a planar structure with the $^2A''$ electronic state and is the most stable among the three open-chain intermediates, 5.0 and 2.9 kcal/mol lower in energy than **21** and **22**, respectively (81.7 kcal/mol below the initial reactants). This stabilization owes to the hydrogen H...O bond between two opposite ends of the chain with the H−O distance of 1.904 Å (see Figure 5). Alternatively, **23** can be formed directly from **10** by the ring opening triggered by rotation of the $(H)CCO_{exo}$ fragment. In this case, the barrier at TS10−23 is 26.4 kcal/mol, 0.3 kcal/mol lower than the barrier at TS10−21.

As seen in Figure 6, the chain isomer **23** can undergo a six-member ring closure via TS23−17 to form the intermediate **17**. At the transition state, the (H)CCO fragment rotates and its C_1 atom is drawn closer to the O_{ring} atom with the C−O distance of 1.876 Å. The C−O bond formation is completed after TS23−17 leading to the six-member ring structure **17** with the CO_{exo} group connected to the ring. The barrier at TS23−17 is calculated to be 29.3 kcal/mol relative to **23**, but the transition state is 52.4 kcal/mol lower in energy than the reactants. **17** easily decomposes to C_5H_5O (pyranyl) + CO (**18**) via TS17−18 by cleaving the out-of-ring C−C bond. The transition state has a rather early character with the breaking C−C bond elongated from 1.593 in **17** to 1.842 Å in TS17−18, and the barrier is only 2.7 kcal/mol relative to **17**. The **17** → C_5H_5O + CO dissociation is exothermic by 17.5 kcal/mol and the final products, pyranyl and carbon monoxide, lie 90.7 kcal/mol below the $C_6H_5 + O_2$ reactants. The overall lowest energy pathway to these products is the following: $C_6H_5 + O_2$ → **1** → **8** → **10** → **23** → **17** → C_5H_5O + CO. After intermediates **1** or **8** are formed at the initial reaction step, the rate-determining step for the production of pyranyl + CO is the **8** → **10** rearrangement (oxygen insertion into the aromatic ring) with TS8−10 residing 27.4 kcal/mol above **1** but 18.9 kcal/mol below the reactants.

Several other, somewhat less favorable, pathways leading from **10** to **17** and therefore to the C_5H_5O + CO products are also possible. First, **10** can directly rearrange to the precursor for CO loss via TS10−17 (see Figure 6). During this process, the C_2-O_{ring} bond in the seven-member ring breaks, while the new C_1-O_{ring} bond is formed to produce a six-member ring structure. The **10** → **17** isomerization is 23.2 kcal/mol endothermic and the transition state exhibits a late character, with the C_2-O_{ring} and C_1-O_{ring} distances for the breaking and forming bonds of 2.441 and 1.937 Å, respectively. The barrier at TS10−17 is 47.5 kcal/mol and the transition state lies 3.5 kcal/mol higher in energy than TS23−17, which is the highest in energy transition state for the **10** → **23** → **17** sequence, thus making the direct **10** → **17** isomerization less favorable than the two-step process.

Alternatively, the open-chain intermediate **21** can undergo ring closure with the formation of a new C−C bond leaving both oxygen atoms in out-of-ring positions and restoring the

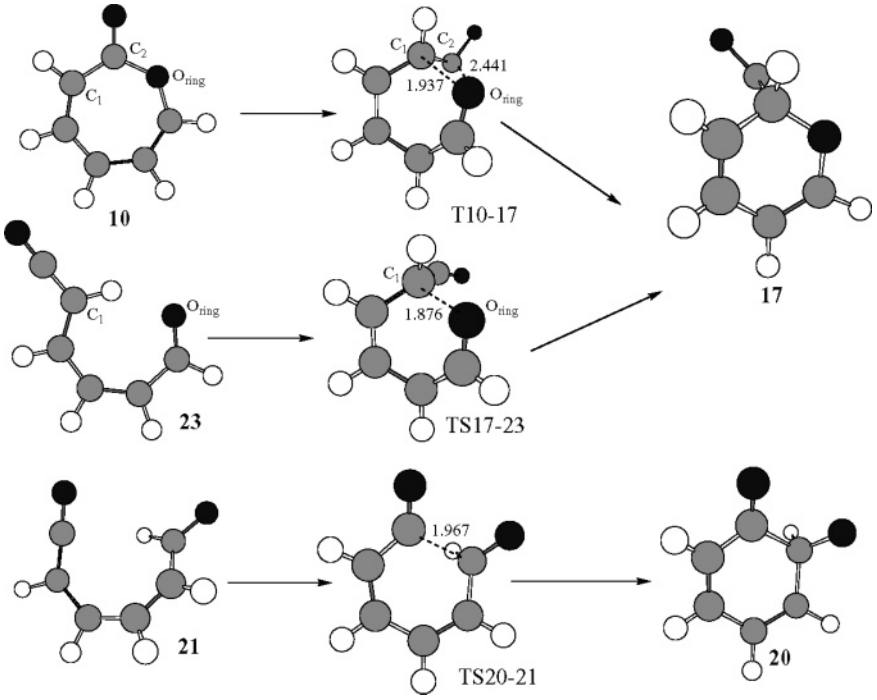

Figure 6. Various ring-closure pathways of the open-chain intermediates.

C_6 aromatic ring (Figure 6). This process occurs via TS20−21 and leads to intermediate **20**, which can be referred to as *o*-$C_6H_4O(O)(H)$ indicating that the two out-of-ring oxygens are located in ortho-position with respect to each other and that there is a C(H)(O) group in one of the ring apexes. Then, the oxygen atom of this group can migrate to occupy a bridging position above the C−C bond in the ring in meta-position relative to the other terminal O atom, producing intermediate **25**, *m*-$C_6H_5O(O)_{br}$. At the G2M level, **20** resides 65.1 kcal/mol below the initial reactants and 3.0 and 3.3 kcal/mol lower in energy than transition-states TS20−21 and TS20−25, separating **20** from the structures **21** and **25**, respectively. The low barrier heights indicate that **20** is likely to be a short-living intermediate. Nevertheless, it is a pivotal intermediate involved in several reaction mechanisms to be discussed in this and subsequent sections. For instance, two pathways lead from **20** to the CO-loss precursor **17** and therefore to the pyranyl + CO products. In the first mechanism, the oxygen atom of the C(H)(O) group in **20** migrates to a position above the carbon ring and forms a new C−O bond with the carbon on the opposite side of the ring, producing intermediate **33**. The latter can be characterized as a bicyclic structure; in addition to the C_6 ring, it also includes a four-member C_3O ring in a different plane. The barrier at TS20−33 is 19.8 kcal/mol relative to **20** and the bicyclic intermediate is 68.2 kcal/mol lower in energy than the initial reactants. At the next step, one of the C−C bonds in the C_6 ring adjacent to the C═O group breaks and the bicyclic structure turns into the C_5O six-member ring with an out-of-ring CO group, that is, intermediate **17**. The barrier between **33** and **17** is calculated to be 15.5 kcal/mol relative to the former.

In the second mechanism, **20** first isomerizes to **25** and then the latter rearranges to 3-oxepinyloxy radical **26** by β-scission of the CC bond of the epoxy ring. The corresponding barrier (at TS25−26) is 17.5 kcal/mol with respect to **25**. Both isomers **26** and **10** have the same oxepinyl ring unit; they differ only in the relative position of the exo- and endocyclyc O atoms, ortho in **10** versus meta in **26**. Nevertheless, the energies of the two isomers are rather different; **26** lies 74.5 kcal/mol below the reactants but 21.9 kcal/mol above **10**, as the latter allows a more effective electron delocalization between its resonance structures (see Chart 1). Subsequently, **26** can rearrange to a bicyclic intermediate **27**, in which one of the C−C bonds in the C_5O cycle is bridged by the CO group. This process occurs by the formation of a new C−C bond between two carbons in **26**, and the barrier is 30.7 kcal/mol. Finally, the CO group in **27** migrates from the bridging to the terminal position breaking one of the C−C bonds it is attached to in the C_5O ring, and structure **17** is produced over a barrier of 15.0 kcal/mol at TS27−17.

CHART 1

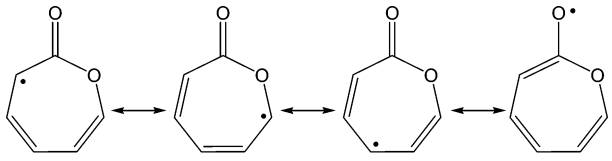

Resonance structures of **10**

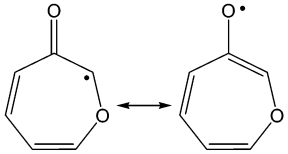

Resonance structures of **26**

When we compare four different mechanisms leading from **10** to the pyranyl + carbon monoxide products via the precursor **17**, **10** → **23** → **17**, **10** → **17**, **10** → **21** → **20** → **33** → **17**, and **10** → **21** → **20** → **26** → **25** → **27** → **17**, we find that the pathway via **23** is the most favorable energetically as the highest in energy transition state on this path, TS23−17, lies 52.4 kcal/mol below the initial reactants. The direct isomerization of **10** to **17** has the transition state 48.8 kcal/mol lower in energy than C_6H_5 + O_2, while the pathway via **33** and those via **26** and **27** exhibit the highest in energy transition states 45.3 (TS20−33) and 38.4 (TS27−17) kcal/mol below the reactants, respectively.

Migration of Oxygen Atom around the Aromatic Ring and Formation of Benzoquinone Products. As we already saw in the previous section, the *o*-$C_6H_4O(O)(H)$ intermediate

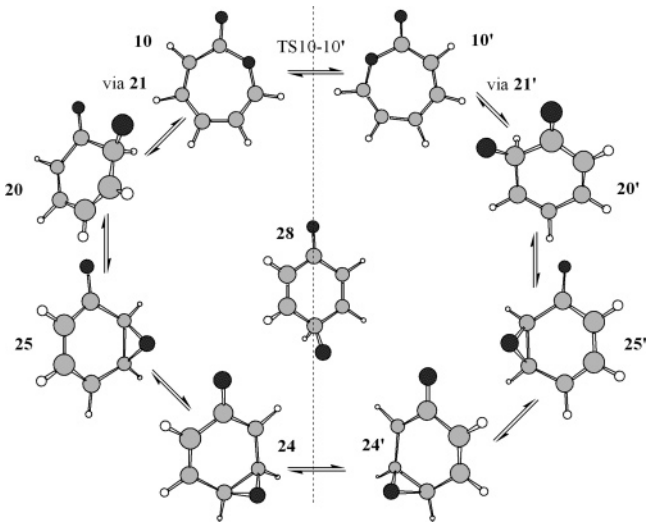

Figure 7. The mechanism of the O-atom migration around the C_6 ring.

20 can be produced from **10** via the open-chain isomer **21**. Fadden et al.[12] also found a transition-state TS10−20 at the B3LYP/6-31G* level, which connects **10** and **20** directly. At the B3LYP/6-311+G**//B3LYP/6-31G* level of theory, TS10−20 lies 9.4 kcal/mol above TS20−21. Although we were able to reproduce the optimized geometry of TS10−20 at B3LYP/6-31G*, at the higher B3LYP/6-311++G** level this transition state does not survive as its optimization converges to TS20−21, indicating that the energetically unfavorable direct pathway from **10** to **20** disappears and this rearrangement can occur only by the two-step mechanism via **21**.

Once the structure **20** is formed, the oxygen atom can continue its migration around the ring. The mechanism of this migration is illustrated in Figure 7, where we show two equivalent directions for the oxygen motion, clockwise and anticlockwise. The meta-bridge isomer **25**, *m*-$C_6H_5O(O)_{br}$, needs to clear a barrier of 50.5 kcal/mol to rearrange to the para-bridge structure *p*-$C_6H_5O(O)_{br}$ **24** via TS25−24 lying 29.2 kcal/mol below the initial reactants. Next, the migrating oxygen atom can reach the most remote para-position with respect to the C═O group, thus forming a structure *p*-$C_6H_4O(O)(H)$ **28** after overcoming a 10.3 kcal/mol barrier at TS24−28. Both **24** and **28** have similar energies and reside ∼71 kcal/mol below the initial reactants but about 9 kcal/mol higher in energy than the meta-bridge isomer **25**. Additional pathways also exist, which lead to **20**, **25**, and **28** directly from the initial intermediate **1** bypassing the seven-member ring structure **10**, but these pathways are much less favorable energetically. For instance, the terminal O atom in the COO group can form a new C−O bond with the adjacent carbon in the ring producing a bicyclic (C_6/C_2O_2) structure **19**. The barrier for this rearrangement is calculated to be 41.3 kcal/mol relative to **1** but the corresponding transition-state TS1−19 is 17.0 and 14.9 kcal/mol, respectively, higher in energy than TS1−8 and TS8−9, the critical transition states on the pathway to the structure **10** and beyond. **19** is a metastable intermediate residing only 8.3 kcal/mol below $C_6H_5 + O_2$, and it is separated from **20** by a very low barrier of 1.6 kcal/mol for the O−O bond cleavage in the four-member C_2O_2 cycle of **19**. Alternatively, the terminal oxygen in **1** can migrate over the area above the aromatic ring leading directly to the meta-bridge isomer **25** or even to the *p*-$C_6H_4O(O)(H)$ structure **28**. However, these processes are highly unfavorable and can be neglected, because the barriers at TS1−25 and TS1−28 are computed to be 104.3 (58.0) and 88.5 (42.2) kcal/mol, respectively, relative to **1** ($C_6H_5 + O_2$).

The *m*-$C_6H_4O(O)(H)$ structure **34** may also exist as a metastable intermediate, 19.4 kcal/mol below the initial reactants but 50−60 kcal/mol higher in energy than the *m*- and *p*-bridge isomers **24** and **25** and the *p*-$C_6H_4O(O)(H)$ structure **28**. A careful search for oxygen migration transition states in the vicinity of **34** shows that it can be produced only from **24** and is separated from the latter by a low barrier of only 1.6 kcal/mol (TS24−34) at the B3LYP/6-311++G** level. At the G2M level, the energy of TS24−34, −27.8 kcal/mol relative to $C_6H_5 + O_2$, is lower than that of **34** indicating that at this level of theory this intermediate is not likely to be a local minimum. From **34**, the system can progress by a 1,2-H shift from the carbon atom of the C(O)(H) group to the neighboring oxygen leading to the structure **35**, which consists of the C_6 ring with a terminal O atom and an OH group. At the G2M level, the H migration barrier is calculated to be 9.0 kcal/mol relative to **34**. If **34** is not a local minimum, **24** rearranges to **35** directly overcoming the barrier of 60.4 kcal/mol at TS34−35. The resulting isomer **35** lies 109.0 kcal/mol lower in energy than $C_6H_5 + O_2$. **35** is an OH-substituted analogue of the phenoxy radical and can, in principle, decompose to C_5H_4OH (OH-substituted cyclopentadienyl) + CO by the mechanism described above for C_6H_5O or be a precursor for the OH group loss to give C_6H_4O + OH. However, the latter channel is highly endothermic and therefore unlikely, because the C_6H_4O (**38**) + OH products reside 103.9 kcal/mol above **35** (5.1 kcal/mol below the initial reactants). The pathway to **35** goes through **25** and **24** and therefore via TS25−24 (only 29.2 kcal/mol below the reactants) and TS34−35 (−10.4 kcal/mol) or TS24−36 (−22.2 kcal/mol) making the formation of **35** in this reaction improbable because many other reaction pathways (for example, those leading to **17** and pyranyl + CO products) have critical transition states significantly lower in energy. Therefore, we do not consider the decomposition mechanism of **35** in detail here. An alternative mechanism to produce **35** proceeds from **24** via intermediate **36** and involves a 1,2-H shift to form a CH_2 group (accompanied with O migration from the para-bridge to meta-position) followed by a 1,3-H migration from the CH_2 group to one of the terminal oxygens. The barriers for these processes are 48.6 and 22.5 kcal/mol relative to **24**. Structure **36** resides in a deep potential well, 108.1 kcal/mol below $C_6H_5 + O_2$, and is only 0.9 kcal/mol less favorable than the isomer **35**. Structures **24** and **28** can undergo some other isomerizations not shown in Figure 1, including, for example, the 1,2-H shift in **28** leading to a para analogue of the OH-substituted phenoxy radical **35** and followed by decomposition of the latter through the CO, H, or OH eliminations or insertion of the bridging O into the C−C bond to produce a para structure similar to the seven-member ring isomers **10** (ortho) and **26** (meta). However, since the formation of **24** and **28** in this reaction is rather unlikely because of the high barrier at TS25−24, we do not pursue these mechanisms further.

The intermediates *o*-$C_6H_4O(O)(H)$ **20** and *p*-$C_6H_4O(O)(H)$ **28** can serve as precursors for the H atom elimination to yield *o*- and *p*-benzoquinones, respectively. For **20**, the H loss appears to be stepwise; the H atom first migrates to make a CH_2 group in intermediate **37** and then is eliminated from the CH_2 group. The transition states for the two steps have similar energies and lie about 52 kcal/mol below the initial reactants. The structure **37** is rather stable, 98.5 kcal/mol below $C_6H_5 + O_2$, and the final products, *o*-$C_6H_4O_2$ + H, are 53.8 kcal/mol exothermic with respect to the reactants. Alternatively, the H atom of the C(H)(O) group in **20** can undergo a 1,2(C,O)-H shift via a barrier of 18.1 kcal/mol relative to **20** to form structure **39**, an analogue

of **35**, an ortho-OH-substituted phenoxy radical. **39** is the most stable structure of all $C_6H_5O_2$ isomers found in this study, 117.7 kcal/mol lower in energy than the reactants. Then, hydrogen elimination from the OH group via TS39−14 leads to the same *o*-$C_6H_4O_2$ + H products. The forward and reverse barriers for the H loss/addition are 67.7 and 3.8 kcal/mol relative to **39** and *o*-$C_6H_4O_2$ + H, respectively. For the para-intermediate **28**, the H elimination process is direct and proceeds via TS28−16 over a 17.1 kcal/mol barrier. The transition state and the products, *p*-$C_6H_4O_2$ + H, lie 53.6 and 61.6 kcal/mol lower in energy than the C_6H_5 + O_2 reactants. Although *p*-benzoquinone is thermodynamically more stable than *o*-$C_6H_4O_2$ (by 7.8 kcal/mol at the G2M level), the former is not likely to be produced in the C_6H_5 + O_2 reaction because of the high barrier on the pathway leading to **28** (at TS25−24). On the other hand, the production of *o*-benzoquinone is probably possible because the relative energy of the critical transition state for this channel, −51.9 kcal/mol (TS14−37), is comparable with the energy of the critical TS on the pathway leading to pyranyl + CO, −52.4 kcal/mol (TS23−17). H eliminations from the C(H)(O) group in **34**, the OH group in **35**, and the CH_2 group in **36** would lead to *m*-benzoquinone; however, such an isomer of $C_6H_4O_2$ does not exist as a stable structure. Therefore, the H losses from **34**−**36** are unlikely to be favorable energetically and are not considered here.

The C_5H_5 + CO_2 Product Channel. Starting from the pivotal intermediate **10**, the reaction can proceed also to the C_5H_5 + CO_2 products. First, the seven-member C_6O ring can fuse into a bicyclic structure **11** consisting of a five-member C_5 and a four-member C_3O rings with a common C−C bond. **11** is almost as stable as **10** and resides 95.0 kcal/mol below the initial reactants. The barrier located at TS10−11 is 34.7 kcal/mol with respect to **10**, but the transition state lies as deep as 61.7 kcal/mol below C_6H_5 + O_2. Two different reaction channels lead from **11** to the cyclopentadienyl radical + carbon dioxide products. In the first mechanism, initially the C−O bond in the four-member cycle breaks to form intermediate **12**. This is followed by the cleavage of the C−C bond connecting the CO_2 group with the C_5H_5 ring resulting in the final products. However, structure **12**, if exists as a local minimum, is a very unstable intermediate. The B3LYP/6-311++G** geometry optimization gives **12** as a stationary point on the PES with all real vibrational frequencies. However, it is only 0.8 and 0.1 kcal/mol more stable than the adjoining transition states TS11−12 and TS12−7, respectively. After ZPE corrections are included into the energies, **12** is still 1.0 kcal/mol more stable than TS11−12 but becomes 0.5 kcal/mol higher in energy than TS12−7. Refinement of the single-point energies at the G2M level gives the relative energy of **12** (−72.0 kcal/mol) higher than those of TS11−12 and TS12−7, −77.0 and −76.4 kcal/mol, respectively. Therefore, **12** is at most a transient structure on the pathway for the CO_2 loss from **11**, and this process is most likely to occur in one concerted step in which both the C−C and C−O bonds attaching CO_2 to the C_5H_5 group are broken together. If **12**, which is the highest in energy structure on the **11** → C_5H_5 + CO_2 pathway, may be considered as a top of the barrier, the C−O bond breaks first, before the barrier, and the C−C bond is cleaved after the barrier is cleared. The second channel leading from **11** to the products initiates by the cleavage of the C−C bond in the four-member ring, which can also be pictured as a rotation of the CO_2 fragment around the O−C bond connecting it to the C_5H_5 ring. As a result, a rather stable intermediate **13** is produced, which possesses C_s symmetry with the mirror plane containing the CO_2 group and the adjacent CH group in the ring. At the next step, the connecting C−O bond is broken and the C_5H_5 + CO_2 products are formed. The barriers for this two-step decomposition of **11** are higher than that for the pathway involving **12**, as the corresponding transition-states TS11−13 and TS13−7 lie 65.3 and 54.4 kcal/mol lower in energy than C_6H_5 + O_2, respectively. Isomer **13** resides in a potential well separated from **11** and C_5H_5 + CO_2 by nonnegligible barriers of 7.2 and 18.1 kcal/mol, respectively.

Finally, there exists a third pathway, which leads from the dioxiranyl radical **8** to the cyclopentadienyl + CO_2 products. This channel proceeds by fusion of the six-member C_6 ring in **8** into five-member and three-member cycles in intermediate **15**, followed by elimination of the CO_2 group. However, the barriers on this pathway are high, 47.3 (15.7) kcal/mol at TS8−15 and 58.9 (27.3) kcal/mol at TS15−7 as counted from **8** (C_6H_5 + O_2), and this reaction channel is not expected to be competitive. C_5H_5 + CO_2 are the most exothermic products as they lie 114.8 kcal/mol lower in energy than the initial reactants. The energetically preferable pathway to these products is **10** → **11** → **12** → C_5H_5 + CO_2 with the highest in energy transition-state TS10−11 residing 61.7 kcal/mol below the reactants. The energy of TS10−11 is about 10 kcal/mol lower than the energies of the critical transition states on the pathways leading to pyranyl + CO (TS23−17, −52.4 kcal/mol) and to *o*-benzoquinone + H (TS14−37, −51.9 kcal/mol). On the basis of these results, we could expect that the branching ratio of the C_5H_5 + CO_2 reaction products should be higher than those for pyranyl and benzoquinone; however, RRKM calculations of multichannel reaction rate constants are required to address this issue quantitatively.

Pathways to the $C_4H_3O_2$ + C_2H_2 Products. Intermediate **12** (although it is established to be only a transient structure) can not only lose the CO_2 group but can also rearrange to another bicyclic structure **32** through the formation of a new O−C bond with the carbon atom in the ring located in the meta position with respect to the out-of-ring C−C bond connecting C_5H_5 with CO_2. On the contrary to **11**, the two five-member rings in **32** are C_5 and C_4O having two common C−C bonds. **32** lies 73.9 kcal/mol below the reactants and the barrier at TS12−32 is 6.1, 8.0, and 29.1 kcal/mol relative to **12**, **32**, and **11**, respectively. At the subsequent reaction step, one of the C−C bonds in the C_5 ring can be broken leading to another intermediate **30**, which has a structure of a C_4O five-member cycle with one out-of-ring oxygen atom and a terminal HCCH group both in the ortho position with respect to the ring O. The transition state corresponding to this rearrangement, TS32−30, resides 46.6 kcal/mol below C_6H_5 + O_2, so the barrier for the C_5-ring opening in **32** is 27.3 kcal/mol. **30** is a precursor for the C_2H_2 elimination; the exocyclic C−C bond can be cleaved overcoming the 22.5 kcal/mol barrier at TS30−31 and resulting in the cyclic C_4OH_3O (2-oxo-2,3-dihydrofuran-4-yl) + acetylene products. These products are computed to be 60.5 kcal/mol exothermic relative to the reactants, and the highest in energy transition state on the **10** → **11** → **12** → **32** → **30** → C_4OH_3O + C_2H_2 pathway is TS30−31 for the final reaction step, which lies 43.5 kcal/mol lower in energy than C_6H_5 + O_2. The energy of this transition state is 18.5 kcal/mol higher than that of TS10−11 (the critical transition state for the **10** → ... → C_5H_5 + CO_2 channel) and 8−9 kcal/mol higher than the energies of TS23−17 (**10** → ... → C_5H_5O (pyranyl) + CO) and TS37−14 (**10** → ... → *o*-$C_6H_4O_2$ (benzoquinone) + H). It is unlikely that such a significant difference in activation enthalpies can be upset by the entropy factor even at high temperatures, so we expect that the contribution of the 2-oxo-2,3-dihydrofuran-4-yl + acetylene

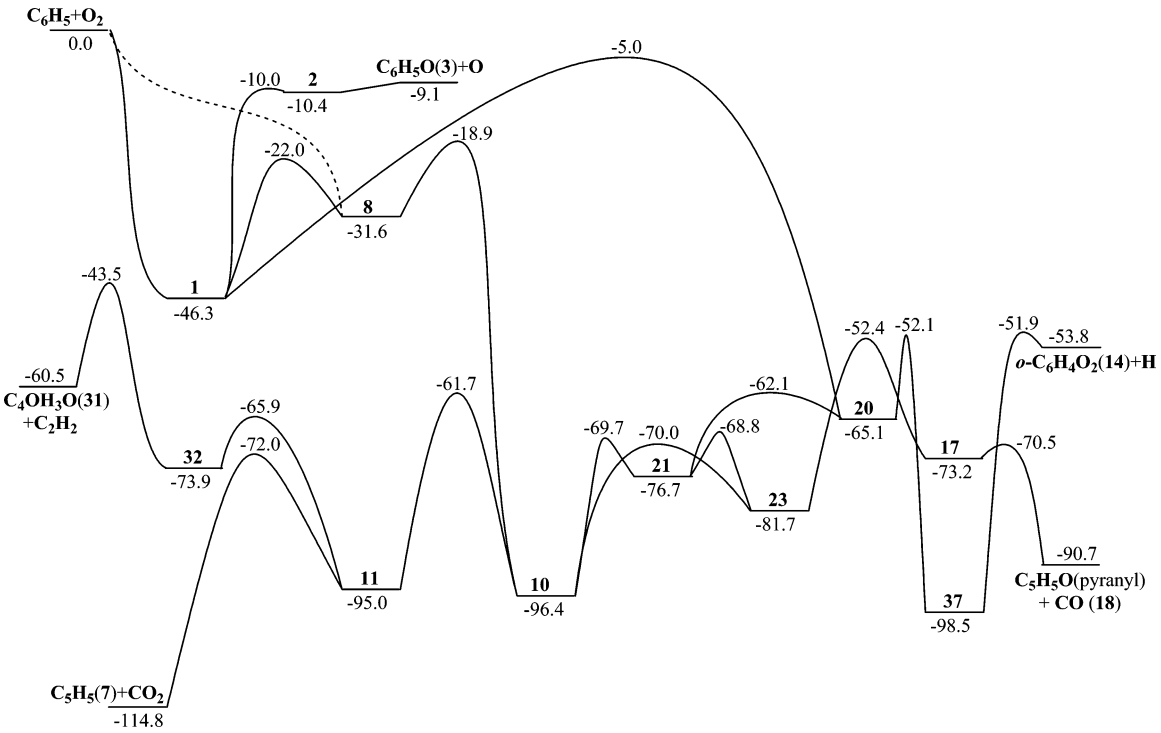

Figure 8. Potential energy diagram for the most important channels of the $C_6H_5 + O_2$ reaction. Relative energies of the reactants, products, intermediates, and transition states are given in kcal/mol as calculated at the G2M level.

product channel should be very minor. Future calculations of rate constants can assess the role of this channel more quantitatively.

Finally, there is one more channel leading to the intermediate **30** and therefore to the $C_4OH_3O + C_2H_2$ products. The C(H)(O) group oxygen atom in the *p*-$C_6H_4O(O)(H)$ structure **28** can migrate to occupy a bridging position roughly above the center of the C_6 ring by forming an extra O−C bond with the carbon on the opposite end of the ring. Such migration produces a bicyclic intermediate **29**, the structure of which can be best described as two five-member C_4O rings with two common C−O bonds. One of these rings can be destroyed by cleaving a single C−C bond and this leads to the structure **30**. However, this process is not expected to be competitive because the transition-states TS28−29, TS29−30, and the intermediate **29** involved lie only 19.8, 34.2, and 39.8 kcal/mol below the initial reactants, and in addition, the structure **28** is not likely to be produced in the first place because of the high barrier at TS25−24. The channel leading to **30** via **11** and **32** is certainly preferable.

Summary of the Most Important Reaction Pathways and Conclusions. A simplified potential energy diagram that summarizes the most important channels of the $C_6H_5 + O_2$ reaction is illustrated in Figure 8. In this diagram, we have included only the energetically favorable channels and have omitted several metastable intermediates, which are not expected to play any role in the reaction kinetics. The reaction starts with a barrierless addition of the oxygen molecule to the radical site of C_6H_5 to produce either phenylperoxy (**1**) or, possibly, dioxiranyl (**8**) radicals with exothermicities of 46.3 and 31.6 kcal/mol, respectively. Next, **1** can lose the terminal oxygen atom and produce the phenoxy + O products, rearrange to **8**, or (less likely) to **25** (via metastable **19** and **20**). The fate of **8** is twofold; it can either isomerize back to the phenylperoxy radical or rearrange to the 2-oxepinyloxy radical **10**, which lies in a deep potential well of 96.4 kcal/mol below the initial reactants. Transformations of **10** in turn give rise to many different reaction products, most importantly, cyclopentadienyl radical + carbon dioxide, pyranyl + carbon monoxide, *o*-benzoquinone + H, and 2-oxo-2,3-dihydrofuran-4-yl (C_4OH_3O) + acetylene. The reaction barriers leading from **10** to this variety of products are much lower than the reverse barrier from **10** to dioxiranyl **8**. Therefore, once **10** is produced, it is unlikely to go back to **8** and **1**, and the branching ratio of $C_6H_5O + O$ against the other products will be mostly controlled by the critical transition-states TS1−2, TS1−8, and TS8−9 (between **8** and **10**). In this regard, the situation here is similar to the vinyl + O_2 reaction, for which the branching ratio between the $C_2H_3O + O$ and other products is mostly governed by the transition states for the COO ring opening and for the O insertion into the C═C bond in the dioxiranylmethyl radical.[21,30,34,35]

According to the calculated energies, in terms of enthalpies, the most favorable product channel for the decomposition of **10** is $C_5H_5 + CO_2$, **10** → **11** → **7** + CO_2, with the highest in energy transition-state TS10−11 residing 61.7 kcal/mol below the initial reactants. This pathway is followed by the channels leading to pyranyl + CO, **10** → **23** → **17** → C_5H_5O + CO, and to *o*-benzoquinone + H, **10** → **21** → **20** → **37** → *o*-$C_6H_4O_2$ + H, with the critical transition states lying about 52 kcal/mol lower in energy than $C_6H_5 + O_2$. Finally, the channel leading to 2-oxo-2,3-dihydrofuran-4-yl + acetylene, **10** → **11** → **32** → ... → $C_4OH_3O + C_2H_2$, has the highest in energy transition-state TS30−31 43.5 kcal/mol below the reactants.

It is well-known from experiment[23−26] and also from theoretical calculations[26,27] that the major products of thermal decomposition of the phenoxy radical C_6H_5O are cyclopentadienyl + carbon monoxide. Since $C_6H_5O + O$ and $C_5H_5 + CO_2$ are expected to be the major primary products of the $C_6H_5 + O_2$ reaction, and C_6H_5O will then decompose to the secondary products $C_5H_5 + CO$, we can conclude here that cyclopentadienyl radicals should be the most important product of oxidation of phenyl radicals by molecular oxygen. Nevertheless, it is important to know the temperature/pressure dependent branching ratios of $C_6H_5O + O$ versus $C_5H_5 + CO_2$ because the primary

C_5H_5 product is formed together with an inert CO_2 molecule, while secondary C_5H_5 (from phenoxy decomposition) is coupled with more reactive CO + O products. The atomic oxygen formed as a primary product of the $C_6H_5 + O_2$ reaction can serve as a chain propagator and oxidize other species in combustion flames.

Taking into account that the C_5H_5 radical is the ultimate product of the phenoxy radical decomposition, as well as a favorable primary product of the $C_6H_5 + O_2$ reaction, the present results demonstrate that the phenyl oxidation reaction primarily leads to degradation of the six-member aromatic ring to the five-member cyclopentadienyl ring, with possible minor contributions of some other products. The C_5H_5 radicals can again serve as precursors for the formation of benzene (for instance, via the $C_5H_5 + CH_3$ reaction),[36] naphthalene (via the self-reaction),[37] or even higher PAHs (for example, via the indenyl + C_5H_5 reaction leading to phenanthrene).[38]

The conclusions concerning the products of the $C_6H_5 + O_2$ reaction and their branching ratios, which we can make here on the basis of the calculated PES, are only preliminary. To predict the product branching ratios and their variation with the temperature and pressure quantitatively, entropic factors need to be taken into account and multichannel RRKM calculations of the reaction rate constants are required. Such calculations based on the reaction mechanism outlined in Figure 8 are now underway in our groups and they will be reported in future publications.

Acknowledgment. This work was funded in part by Academia Sinica and National Science Council of Taiwan and in part by the Chemical Sciences, Geosciences and Biosciences Division, Office of Basic Energy Sciences, Office of Sciences of the U.S. Department of Energy (Grant No. DE-FG02-04ER15570 to FIU and Grant No. DE-FG02-97ER14784 to Emory University).

Supporting Information Available: Calculated total energies, ZPE, moments of inertia, rotational constants, optimized Cartesian coordinates, and vibrational frequencies of all intermediates and transition states involved in the $C_6H_5 + O_2$ reaction (Table S1). This material is available free of charge via the Internet at http://pubs.acs.org.

References and Notes

(1) Glassman, I. *Combustion*, 2nd ed.; Academic Press: New York, 1986.

(2) Brezinsky, K. *Prog. Energy Combust. Sci.* **1986**, *12*, 1.

(3) Bittker, D. A. *Combust. Sci. Technol.* **1991**, *79*, 49.

(4) Bittner, J. D.; Howard, J. B.; Palmer, H. B. *NATO Conference Series, 6: Materials Science;* Plenum Press: New York, 1983; Vol. 7, p 95.

(5) Colussi, A. J.; Zabel, F.; Benson, S. W. *Int. J. Chem. Kinet.* **1977**, *9*, 161.

(6) Lin, C.-Y.; Lin, M. C. *J. Phys. Chem.* **1986**, *90*, 425.

(7) (a) Herzler, J.; Frank, P. *Third International Conference on Chemical Kinetics*, NET, Gaithersburg, MD, July 12−16, 1993. (b) Frank, P.; Herzler, J.; Just, Th.; Wahl, C. *Proceedings of the 25th International Symposium on Combustion*; The Combustion Institute: Pittsburgh, PA, 1994; p 833.

(8) Yu, T.; Lin, M. C. *J. Am. Chem. Soc.* **1994**, *116*, 9571.

(9) Carpenter, B. K. *J. Am. Chem. Soc.* **1993**, *115*, 5, 9806; *J. Phys. Chem.* **1995**, *99*, 9801.

(10) Mebel, A. M.; Lin, M. C. *J. Am. Chem. Soc.* **1994**, *116*, 9577.

(11) Lin, M. C.; Mebel, A. M. *J. Phys. Org. Chem.* **1995**, *8*, 407.

(12) (a) Fadden, M. J.; Barckholtz, C.; Haddad, C. M. *J. Phys. Chem. A* **2000**, *104*, 3004. (b) Fadden, M. J.; Hadad, C. M. *J. Phys. Chem. A* **2000**, *104*, 8121. (c) Merle, J. K.; Hadad, C. M. *J. Phys. Chem. A* **2004**, *108*, 8419.

(13) (a) Becke, A. D. *J. Chem. Phys.* **1992**, *96*, 2155. (b) Becke, A. D. *J. Chem. Phys.* **1992**, *97*, 9173. (c) Becke, A. D. *J. Chem. Phys.* **1993**, *98*, 5648. (d) Lee, C.; Yang, W.; Parr, R. G. *Phys. Rev.* **1988**, *B37*, 785.

(14) (a) Gonzalez, C.; Schlegel, H. B. *J. Chem. Phys.* **1989**, *90*, 2154. (b) Gonzalez, C.; Schlegel, H. B. *J. Phys. Chem.* **1990**, *94*, 5523.

(15) Mebel, A. M.; Morokuma, K.; Lin, M. C. *J. Chem. Phys.* **1995**, *103*, 7414.

(16) (a) Knowles, P. J.; Hampel, C.; Werner, H. J. *J. Chem. Phys.* **1993**, *99*, 5219−5227 and references therein. (b) Knowles, P. J.; Hampel, C.; Werner, H. J. *J. Chem. Phys.* **2000**, *112*, 3106-7. (c) Watts, J. D.; Gauss, J.; Bartlett, R. J. *J. Chem. Phys.* **1993**, *98*, 8718.

(17) Cramer, C. J. *Essentials of Computational Chemistry. Theories and Models*; Wiley: New York, 2002.

(18) Frisch, M. J.; Trucks, G. W.; Schlegel, H. B.; Scuseria, G. E.; Robb, M. A.; Cheeseman, J. R.; Zakrzewski, V. G.; Montgomery, J. A.; Stratmann, R. E.; Burant, J. C.; Dapprich, S.; Millam, J. M.; Daniels, R. E.; Kudin, K. N.; Strain, M. C.; Farkas, O.; Tomasi, J.; Barone, V.; Cossi, M.; Cammi, R.; Mennucci, B.; Pomelli, C.; Adamo, C.; Clifford, S.; Ochterski, J.; Petersson, G. A.; Ayala, P. Y.; Cui, Q.; Morokuma, K.; Salvador, P.; Dannenberg, J. J.; Malick, D. K.; Rabuck, A. D.; Raghavachari, K.; Foresman, J. B.; Cioslowski, J.; Ortiz, J. V.; Baboul, A. G.; Stefanov, B. B.; Liu, G.; Liashenko, A.; Piskorz, P.; Komaromi, I.; Gomperts, R.; Martin, R. L.; Fox, D. J.; Keith, T.; Al-Laham, M. A.; Peng, C. Y.; Nanayakkara, A.; Challacombe, M.; Gill, P. M. W.; Johnson, B.; Chen, W.; Wong, M. W.; Andres, J. L.; Gonzalez, C.; M. Head-Gordon, M.; Replogle, E. S.; Pople, J. A. *Gaussian 98*, revision A.11; Gaussian, Inc.: Pittsburgh, PA, 2001.

(19) Frisch, M. J.; Trucks, G. W.; Schlegel, H. B.; Scuseria, G. E.; Robb, M. A.; Cheeseman, J. R.; Montgomery, J. A., Jr.; Vreven, T.; Kudin, K. N.; Burant, J. C.; Millam, J. M.; Iyengar, S. S.; Tomasi, J.; Barone, V.; Mennucci, B.; Cossi, M.; Scalmani, G.; Rega, N.; Petersson, G. A.; Nakatsuji, H.; Hada, M.; Ehara, M.; Toyota, K.; Fukuda, R.; Hasegawa, J.; Ishida, M.; Nakajima, T.; Honda, Y.; Kitao, O.; Nakai, H.; Klene, M.; Li, X.; Knox, J. E.; Hratchian, H. P.; Cross, J. B.; Adamo, C.; Jaramillo, J.; Gomperts, R.; Stratmann, R. E.; Yazyev, O.; Austin, A. J.; Cammi, R.; Pomelli, C.; Ochterski, J.; Ayala, P. Y.; Morokuma, K.; Voth, G. A.; Salvador, P.; Dannenberg, J. J.; Zakrzewski, V. G.; Dapprich, S.; Daniels, A. D.; Strain, M. C.; Farkas, O.; Malick, D. K.; Rabuck, A. D.; Raghavachari, K.; Foresman, J. B.; Ortiz, J. V.; Cui, Q.; Baboul, A. G.; Clifford, S.; Cioslowski, J.; Stefanov, B. B.; Liu, G.; Liashenko, A.; Piskorz, P.; Komaromi, I.; Martin, R. L.; Fox, D. J.; Keith, T.; Al-Laham, M. A.; Peng, C. Y.; Nanayakkara, A.; Challacombe, M.; Gill, P. M. W.; Johnson, B.; Chen, W.; Wong, M. W.; Gonzalez, C.; Pople, J. A. *Gaussian 03*, Revision B.01; Gaussian, Inc.: Pittsburgh, PA, 2003.

(20) Amos, R. D.; Bernhardsson, A.; Berning, A.; Celani, P.; Cooper, D. L.; Deegan, M. J. O.; Dobbyn, A. J.; Eckert, F.; Hampel, C.; Hetzer, G.; Knowles, P. J.; Korona, T.; Lindh, R.; Lloyd, A. W.; McNicholas, S. J.; Manby, F. R.; Meyer, W.; Mura, M. E.; Nicklaβ, A.; Palmieri, P.; Pitzer, R.; Rauhut, G.; Schütz, M.; Schumann, U.; Stoll, H.; Stone, A. J.; Tarroni, R.; Thorsteinsson, T.; Werner, H.-J. *MOLPRO*, version 2002.6; University of Birmingham: Birmingham, U.K., 2003.

(21) Mebel, A. M.; Diau, E. W. G.; Lin, M. C.; Morokuma, K. *J. Am. Chem. Soc.* **1996**, *118*, 9759.

(22) The best experimental enthalpies of formation are $\Delta_fH_0°(O) = 59.0$ kcal/mol, $\Delta_fH_0°(C_6H_5) = 83.7 \pm 0.6$ kcal/mol [Ervin, K. M.; DeTuri, V. F. *J. Phys. Chem. A* **2002**, *106*, 9947], $\Delta_fH_0°(C_6H_5O) = 16.5 \pm 1.4$ kcal/mol [$\Delta_fH_{298}°$ from Tsang, W. Energetics of Organic Free Radicals. In *Energetics and Reactivity in Chemistry Series (SEARCH)*; Simoes, J. A., Greenberg, A., Liebman, J. F., Eds.; Chapman and Hall: London, 1996; and thermal correction from Janoschek, R.; Rossi, M. J. *Int. J. Chem. Kinet.* **2002**, *34*, 550]. These give -8.2 ± 2.0 kcal/mol for the heat of reaction.

(23) Lin, C.-Y.; Lin, M. C. *Int. J. Chem. Kinet.* **1985**, *17*, 1025; *J. Phys. Chem.* **1986**, *90*, 425.

(24) Colussi, A. J.; Zabel, F.; Benson, S. W. *Int. J. Chem. Kinet.* **1977**, *9*, 161.

(25) Harrison, A. G.; Honnen, L. R.; Dauben, H. J.; Lossing, F. P. *J. Am. Chem. Soc.* **1960**, *82*, 5593.

(26) Schmoltner, A.-M.; Anex, D. S.; Lee, Y. T. *J. Phys. Chem.* **1992**, *96*, 1236.

(27) Olivella, S.; Sole, A.; Garcia-Raso, A. *J. Phys. Chem.* **1995**, *99*, 10549.

(28) Liu, R.; Morokuma, K.; Mebel, A. M.; Lin, M. C. *J. Phys. Chem.* **1996**, *100*, 9314.

(29) A more detailed description of the electronic states of **9** can be given, in principle, in terms of the three-electrons-in-three-orbitals model [Slipchenko, L. V.; Krylov, A. I. *J. Chem. Phys.* **2003**, *118*, 9614; another example is described in Slipchenko, L. V.; Munsch, T. E.; Wenthold, P. G.; Krylov, A. I. *Angew. Chem., Int. Ed.* **2004**, *43*, 742]. These works show, in particular, that three nearly degenerate triradical orbitals result in one quartet state and eight multiconfigurational doublet states.

(30) Carpenter, B. K. *J. Phys. Chem. A* **2001**, *105*, 4585.
(31) Sølling, T. I.; Smith, D. M.; Radom, L.; Freitag, M. A.; Gordon, M. S. *J. Chem. Phys.* **2001**, *115*, 8758.
(32) Mebel, A. M.; Kislov, V. V., submitted to *J. Phys. Chem. A.*
(33) Lee, T. J.; Taylor, P. R. *Int. J. Quantum Chem.* **1989**, *S23*, 199.
(34) Carriere, T.; Westmoreland P. R.; Kazakov, A.; Stein Y. S.; Dryer, F. L. *Proc. Int. Symp. Combust.* **2002**, *29*, 1257.
(35) Miller, J. A. *Faraday Discuss.* **2001**, *119*, 461.
(36) Moskaleva, L. V.; Mebel, A. M.; Lin M. C. *Proc. Int. Symp. Combust.* **1996**, *26*, 521.
(37) Melius, C. F.; Colvin, M. E.; Marinov, N. M.; Pitz, W. J.; Senkan, S. M. *Proc. Int. Symp. Combust.* **1996**, *26*, 685.
(38) Marinov, N. M.; Pitz, W. J.; Westbrook, C. K.; Vincitore, A. M.; Castaldi, M. J.; Senkan, S. M.; Melius, C. F. *Combust. Flame* **1998**, *114*, 192.